Major parameter measurement of high-brightness injector in Hefei Light Source

WANG Xiaohui HE Zhigang SUN Baogen* JIA Qika

School of Nuclear Science and Technology & National Synchrotron Radiation Laboratory, University of Science and Technology of China, Hefei 230029, China

Abstract A photocathode radio frequency gun, which is an S-band normal conducting 1.6 copper cell cavity with water cooling system, was installed in Hefei Light Source. In order to know its characteristics and get it into normal operation, continuous conditioning was conducted in the last few months. Beam charge and dark current charge were measured using integrating current transformer. The beam transverse size was determined as 1.63 mm in minimum using YAG screen and GigE Vision camera. Using multi-slits technique, the transverse emittance was measured and normalized at 1.95 mm·mrad with beam charge of 240 pC. The results provide a way to optimize the facility.

Key words Photocathode RF gun, Transverse emittance, Beam charge, Solenoid

1 Introduction

High-brightness injector with photocathode radio frequency (RF) gun plays an important role in free electron laser (FEL), future linear collider, Thomson scattering X-ray light source[1] and other scientific applications[2]. A new photocathode RF gun was installed in Heifei Light Source (HLS) in 2009. The gun is an S-band normal conducting 1.6 copper cell cavity with water cooling system. With a center frequency of 2856 MHz and the maximum gradient of 100 MV/m at 10 MW peak power, the Nd:YLF laser can be driven to emit electrons. The forth harmonic (262-nm) of fundamental 1047 nm is generated with frequency conversion crystals. In longitudinal direction, the laser pulse shape is Gaussian with the full width at half maximum (FWHM) of 8.3 ps. The root mean square (RMS) laser spot size in (x, y) plane is 0.5 mm. The laser is of 10 Hz repetition. However, because of limitations in vacuum conditions and klystron power supply controller, the RF pulse repetition is set to 1 Hz. Therefore, the repetition of electron beam is 1 Hz.

2 Conditioning of the gun

During conditioning of the gun, which lasted for a few months, the RF pulse length was fixed at 4 μs, and the setup time of the electromagnetic field in the gun was about 1 μs. High voltage (HV) set point in klystron power supply controller increased step by step due to the limitation of vacuum conditions to observe the RF power at the exit of the klystron (Fig.1).

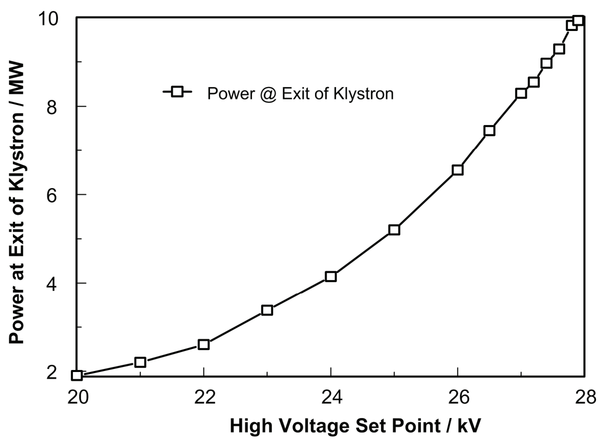

Fig.1 Conditioning of the high-brightness injector of HLS.

Supported by the Natural Science Foundation of China (10875117), the National “985 Project” (173123200402002) and the China Scholarship Council (Grant No. 2009634063).

* Corresponding author. *E-mail address*: bgsun@ustc.edu.cn

Received date: 2011-03-25

2.1 Initial measurement results

When the gun was emitting electrons, beam diagnostics was used to check the gun status, i.e. the beam charge, transverse size and transverse emittance, and components of the high-brightness injector were arranged (Fig.2)[3].

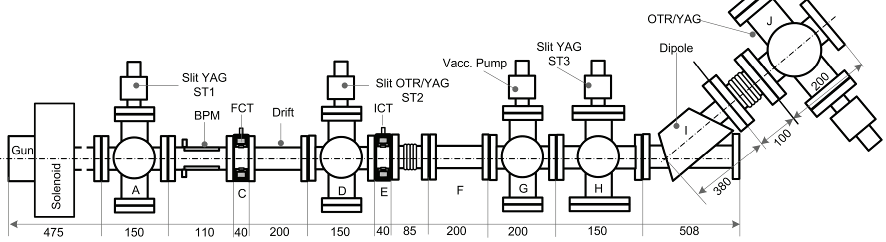

Fig.2 Layout of the high-brightness injector in HLS.

2.2 Beam charge measurement

The beam charge and dark current were measured without interruption using integrating current transformer (ICT)[4] (Bergoz Company). Specifications of the ICT are given in Table 1. The ICT output pulse was stretched to 70 ns to observe 500-MHz bandwidth on an oscilloscope (Fig.3).

Table 1 Specifications of the integrating current transformer.

Input current rise time / ps	< 1
Linearity error /%	< 10
Droop in 50-Ω load / μs	< 10%
Output rise time / ns	~ 30
Output pulse duration / ns	~ 70

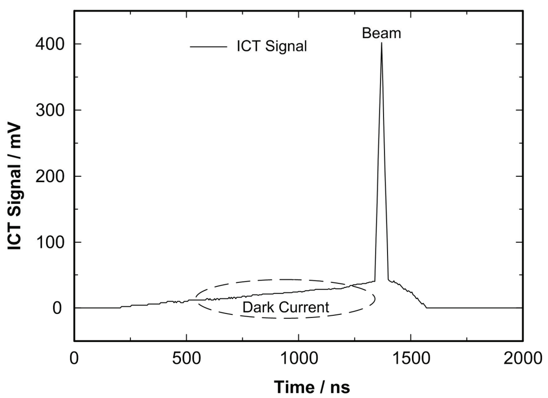

Fig.3 Output signal of ICT.

The beam charge was calculated by integrating the output signal. The charge of dark current and beam was about 760 and 180 pC at the laser energy of about 90 μJ. The charge of dark current in the gun, a key parameter[5], is systematically measured (Fig.4). It varies with the solenoid current at different RF power levels, and results in its focus or defocus. At focus, it fully passes through the ICT with high output, while at defocus, some of the electrons crash into the vacuum pipe, yielding small output in the ICT. The peak dark current increases with HV set point due to referring to RF power level. In our case, copper is used as cathode material, and its quantum efficiency is obtained by linear fitting of the beam charge as a function of laser energy (Fig.5).

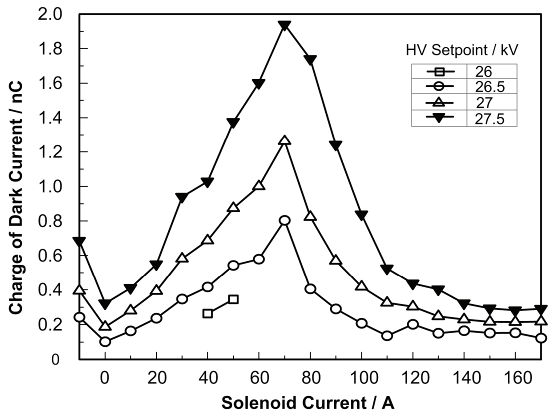

Fig.4 Charge of dark current as a function of solenoid current.

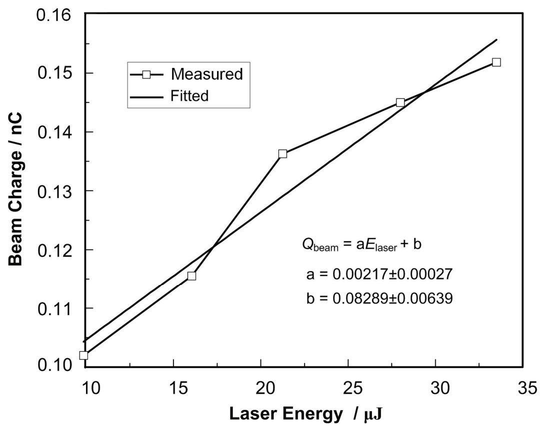

Fig.5 Quantum efficiency of RF gun in HLS.

The slope of the linear fitting is 2.17×10^{-6} C/J at exit energy of the laser system. The laser beam losses should be taken into consideration. At the gun entrance, the laser beam has a 10% loss because of the absorption and scattering by the mirrors and dust in the air, and a 20% loss because of reflection from the cathode surface. Therefore, the gun quantum efficiency is 3.1×10^{-6} C/J. The quantum efficiency is the number of the generated electrons over the photon number, which is 1.47×10^{-5} C/J at 262 nm laser.

With the material of the same efficiency, the beam charge is proportional to the laser energy. So a 1-nC beam charge requires laser energy of 460 μJ. However, the maximum energy of 650-μJ set up in the laser system was less than 200 μJ and changed often during measurement.

Applying this quantum efficiency to Fig.3, the laser energy is 90 μJ. This means a beam charge of over 270 pC, but the real value is 180 pC. This is because Fig.3 was measured when the injector was commissioned, and Fig.5 was measured four months later. After the injector commission, however, the gun was exposed to the air and the copper surface might be oxidized. During conditioning, the laser repetition was higher than that of beam, and the laser beams which did not produce electrons was used to clean the cathode surface.

Also, the dust in the air from exit of laser system to the entrance of the gun may cause the laser beam loss. A mask is being designed to minimize the dust effect.

The video system (Fig.6) consists of mainly the YAG laser and screen, a GigE vision camera[6], and a PC. A pattern of known dimensions was used to determine zoom factor of the camera. It also has an OTR laser, which is much less powerful than YAG laser. During the conditioning, we used the YAG only. The images are captured by a GigE vision camera[6], and the data were transported via a gigabit network. When the camera was mounted, the lens was focus on the screen in the vacuum pipe. The mirror was inserted, the pattern-mirror distance was adjusted, the camera was focused on the pattern, and the camera's zoom factor was measured at 0.081 mm/pixel at the first screen, which is 0.55 m downstream from the gun. The beam transverse size, which is defined as $\sigma_{xy}=(\sigma_x\sigma_y)^{0.5}$, varied with the current of scanning solenoid, as shown in Fig.7, where the simulation results were done at 30 MV/m using ASTRA[7].

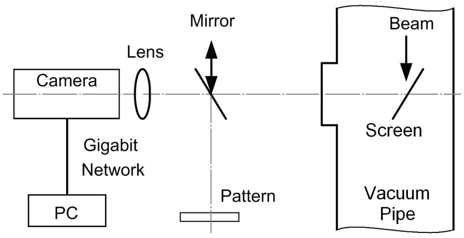

Fig.6 Layout of video system in the high-brightness injector.

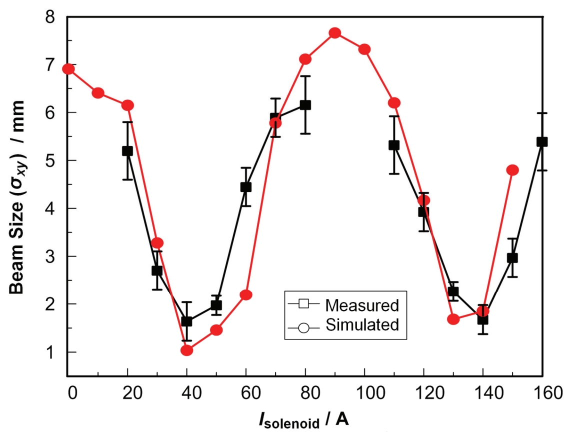

Fig.7 Transverse beam size vs current of scanning solenoid at the first screen.

3 Transverse emittance measurement

Performance of an accelerator driven FEL facility is determined by emittance of electron beam, which is a key factor deserves theoretical and experimental investigations. Multi-slit-based emittance measurement[8] was used in the high-brightness injector.

The slit width (d), slit separation (w), slit thickness (t), and drift length (L) are crucial for multi-slit emittance measurement[9]. The slit width (d) should be small enough to make the beamlets emittance-dominated, while ensuring enough electrons to pass through for signal detection. At a certain beam spot, a small slit separation produces more precise beamlets, hence a higher precision calculation, but it should not cause overlapped beamlets. The slit should be thick enough to prevent electrons from penetrating the slit plate, but if it is too thick, the acceptance angle would be smaller than what is required. A long drifting length benefits signal detection, whereas the beamlets overlapping increases with L. For these reasons, the experiments were performed with SS multislits of d =90 μm, w =1.0 mm, t =2.0 mm, and L =500 mm.

When capturing the beamlet image, geometric emittance of the electron beam at the multi-slits is extracted by the following steps. The beam centroid at the multi-slits plane is

$$\langle x\rangle = \frac{1}{N}\sum_{j=1}^{p} n_j x_{sj} \tag{1}$$

where, N is the number of electrons passing through the multi-slits, x_{sj} is the position of j^{th} slit (j = 1, 2, …, p), n_j is the number of electrons passing the j^{th} slit. The root mean square (RMS) spread of the beam is

$$\langle x^2\rangle = \frac{1}{N}\sum_{j=1}^{p} n_j \left(x_{sj} - \langle x\rangle\right)^2 \tag{2}$$

and the average divergence is

$$\langle x'\rangle = \frac{1}{N}\sum_{j=1}^{p} n_j \langle x_j'\rangle \tag{3}$$

where, $<x_j'>$ is the average divergence of j^{th} beamlet at the multi-slits plane.

$$\langle x_j'\rangle = \frac{\langle X_{sj}\rangle - x_{sj}}{L} \tag{4}$$

where, $<X_{sj}>$ is the average position of the j^{th} beamlet at the detection plane. The RMS spread in divergence for the j-th beamlet is

$$\sigma_j' = \sigma_j / L \tag{5}$$

Then, the RMS spread in divergence for the beam at the multi-slits plane cab be obtained by

$$\langle x'^2\rangle = \frac{1}{N}\sum_{j=1}^{p}\left[n_j \sigma_j'^2 + n_j\left(\langle x_j'\rangle - \langle x'\rangle\right)^2\right] \tag{6}$$

The beam emittance at the multi-slits plane is

$$\varepsilon = \sqrt{\langle x^2\rangle\langle x'^2\rangle - \langle xx'\rangle^2} \tag{7}$$

where

$$\langle xx'\rangle = \frac{1}{N}\left(\sum_{j=1}^{p} n_j x_{sj}\langle x_j'\rangle - N\langle x\rangle\langle x'\rangle\right) \tag{8}$$

According to Eqs.(1)–(8), the geometric emittance of beam is 0.65 mm·mrad with the beam charge of 240 pC at laser energy of about 80 μJ (Fig.8). And the normalized emittance, defined as $\varepsilon_{Norm} = \beta\gamma\varepsilon$, is 1.95 mm·mrad at the beam energy of 1.53 MeV.

In order to overcome the overlapping between adjacent beamlets, the distribution of each beamlet was obtained by Gaussian fitting, especially the left beamlet was subtracted from the entire distribution to yield a new distribution.

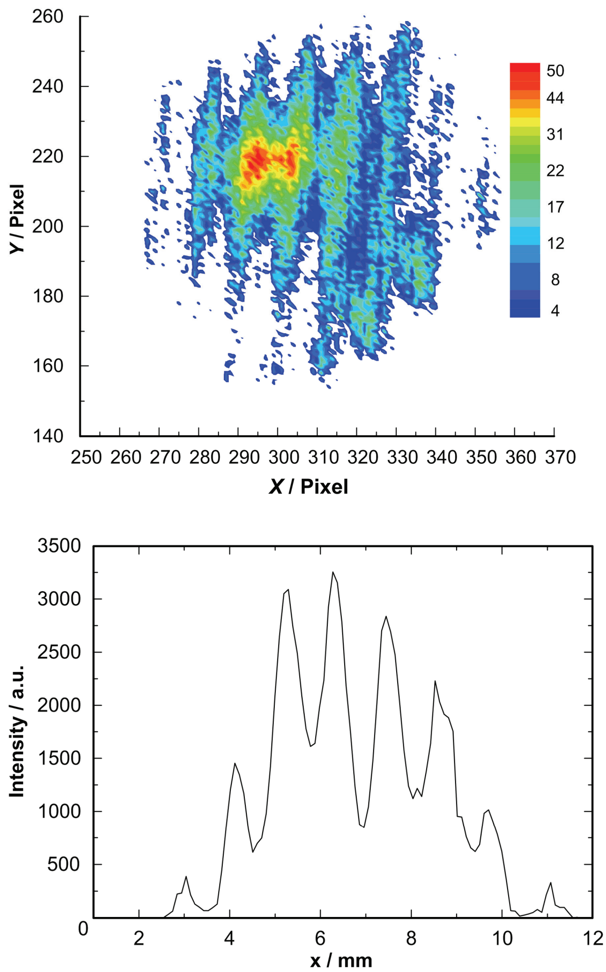

Fig.8 Beamlets passing vertical multislits and the projection.

4 Conclusions

After conditioning for a few months, about 10 MW of the gun power was achieved, and it is close to the full operation power. The charge of dark current and beam was measured without interruption by using ICT. The minimum transverse beam size was 1.63 mm observed by the YAG screen and GigE Vision camera. The normalized emittance is 1.95 mm·mrad at beam charge of 240 pC. The results do not meet our final goal, but they provide a way to optimize the facility.

References

1 Gibson D J, Anderson S G, Barty C P J, *et al.* Phys Plasmas, 2004, **11:** 2857–2864.

2 Neumann J, Fiorito R, Freund H, *et al.* Generation of Terahertz Radiation by Modulating the Electron Beam at the Cathode. Proceedings of the 2004 FEL Conference, Trieste, Italy, 2004, 9, 586–589.

3 Wang X H, Sun B G, Lu P, *et al.* Design of Beam Measurement System for High Brightness Injector in HLS. Proceedings of PAC 2009, Vancouver, Canada, 2009, 5, 4090–4092.

4 Unser K B. Design and Preliminary Tests of a Beam Intensity Monitor for LEP. Proceedings of the 1989 IEEE Accelerator Conference, Chicago, USA, 1989, **1(3):** 71–73.

5 Otevrel M, Asova G, Bähr J W, *et al.* Conditioning of A New Gun at PITZ Equipped with An Upgraded RF Measurement System. Proceedings of the 2010 FEL conference, Malmö, Sweden, 2010, 8, 398–401.

6 Tang L L, Sun B G, Wang J G, *et al.* Application of the Gige Vision Digital Camera for Beam Diagnostics in HLS. Proceedings of IPAC 2010, Kyoto, Japan, 2010.5, 1041–1043.

7 Flöttmann K, http://www.desy.de/~mpyflo/(September 8, 2010).

8 Anderson S G, Rosenzweig J B, Lesage G P, *et al.* Emittance Measurements of the Space Charge Dominated Thomson Source Photoinjector. Proceedings of PAC 2001, Chi-cago, USA, 2001.6, 2260–2262.

9 Rosenzweig J, Travish G. Nucl Instrum Meth,1994, **A341:** 379–385.